Gait Distinction via Hip-Knee Coordination:

Applications of Dynamical Systems Theory & Computational Topology

Zafar, Abdullah
999730411

Computational Physics
PHY407, Fall 2020
University of Toronto

December 18, 2020

Contents

1 Introduction **3**
- 1.1 Phase Space . . . 3
- 1.2 Continuous Relative Phase . . . 3
- 1.3 Algebraic Topology . . . 3
  - 1.3.1 Simplicial Complex . . . 3
  - 1.3.2 Homology Groups . . . 4

2 Computational Background **5**
- 2.1 Computing Persistent Homology . . . 5
  - 2.1.1 Vietoris-Rips Filtrations . . . 5
  - 2.1.2 Boundary Matrices . . . 5
  - 2.1.3 Homology Intervals . . . 6
- 2.2 Topological Approximation via Witness Complexes . . . 6
- 2.3 Wasserstein Distance . . . 6

3 Methods **6**
- 3.1 Dataset . . . 6
- 3.2 Continuous Relative Phase Analysis . . . 7
- 3.3 Clustering Gait Patterns . . . 7

4 Results & Analysis **9**
- 4.1 Results . . . 9
- 4.2 Analysis . . . 10

5 Discussion **11**

6 Conclusion **11**

References **12**

APPENDIX I: Algorithms **13**

1 Introduction

1.1 Phase Space

In applications of classical mechanics (like biomechanics) the state of a body can be described by its position and momentum; that is, the state space can be embedded in $\mathbb{R}^2$, where one dimension is position (x) and the other dimension is velocity ($\dot{x}$) - such a space is typically referred to as the *phase space* (see Figure 1 for an example using a simple pendulum). The phase space of a body encodes important information about the overall behaviour of the system.

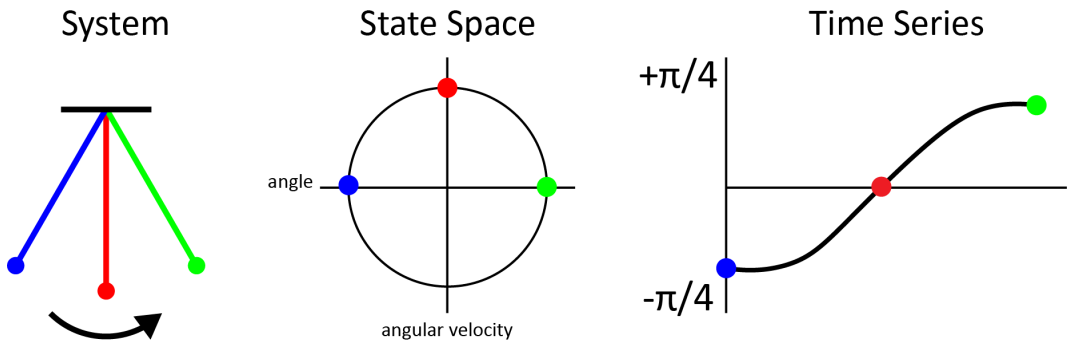

Figure 1: A simple pendulum *(left)*, its corresponding representation as a state (i.e. phase) space *(middle)* and as a position-time time series *(right)*

In particular, *attractors* of the system (states or behaviours that the system tends towards) are identifiable from the phase space of the system. In relation to biomechanics, two types of attractors are of interest: the fixed point attractor and the limit cycle. The fixed point attractor represents a particular state that the system tends towards and remains in, for some time at least; such attractors can be identified either by trajectories in the phase space asymptotically approaching a single point (like in a spiral), or by having trajectories clustering together about a particular point; this former phenomenon indicates the system has entered the "basin of attraction" for the fixed point attractor, although it may not converge completely to a single state. By contrast, the limit cycle represents periodic behaviour in the system - it does not completely converge to a single state, nor does it completely diverge; such attractors are easily identifiable as literal loops forming in the phase space.

1.2 Continuous Relative Phase

In the biomechanical analysis of whole body movements, continuous relative phase is a measure used to quantify the coordination between a pair of joints of the body [1]. The method considers the two joints as a pair of pendulums, each with a circular phase space constructed using the joint angle and joint angular velocity. In practice, the phase space will not be circular, but perhaps more elliptical and so the joint angles and angular velocities must be normalized before constructing the phase space. Once the phase space is normalized, each point on the phase plane can be represented by a phase angle - the angle the point makes with the origin, i.e. $\theta(t_i) = arctan(\frac{\dot{x}_{norm}(t_i)}{x_{norm}(t_i)})$.

Finally, the continuous relative phase (CRP) angle at time t becomes the difference in the phase angle of both joints. Such an angle may be reported in the range of 0 to 2π or $-\pi$ to $+\pi$. Regardless, multiples of π imply limbs are *in-phase* with each other.

1.3 Algebraic Topology

1.3.1 Simplicial Complex

A simplicial complex can be formally defined as a finite collection of sets S such that $\forall \alpha \in S$ and $\beta \subseteq \alpha$, then $\beta \in S$. Geometrically we might understand this as follows: a 0-dimensional simplex is a point, a 1-dimensional simplex is a line, a 2-dimensional simplex is a triangle, a 3-dimensional simplex is a tetrahedron, and so on. Each lower dimensional simplex is a *face* (a "building block") of a higher

dimensional simplex, and all possible combinations of lower dimensional simplices are contained in a higher dimensional simplex.

Take the example of a square and a triangle, as in Figure 2: the square is not a simplex, while the triangle is. The square is made of 4 vertices, but not all combinations of vertices are connected (i.e. become the higher dimensional 1-simplex, a line) - namely, there are no lines connecting the diagonals. By contrast, the triangle is a simplex because all possible combinations of vertices form the 1-dimensional lines in the shape.

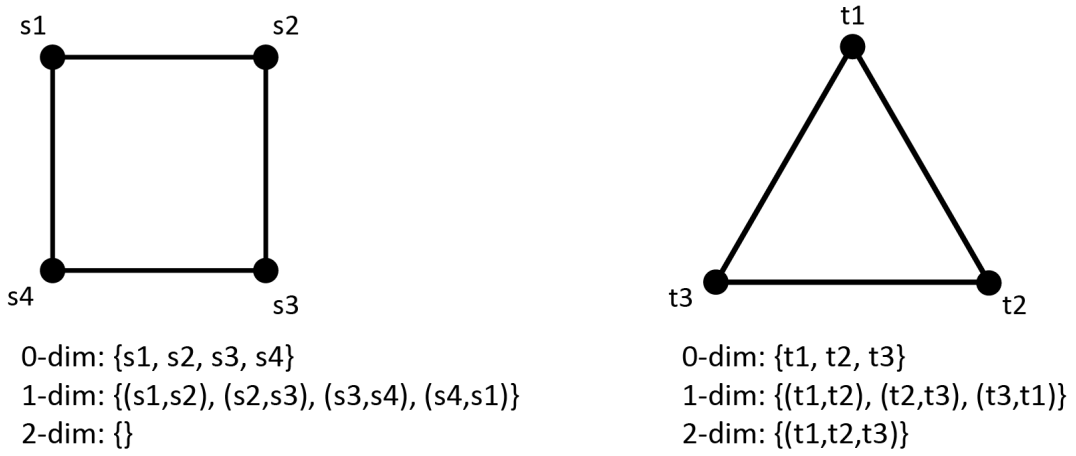

Figure 2: The triangle *(right)* is a 2-dimensional simplex, while the square *(left)* is not

A simplicial complex is then a collection of these simplices (i.e. points, lines, triangles, tetrahedrons, etc.), which are either not connected at all or connect along a *face* (i.e. a point, an edge, a face, and so on).

1.3.2 Homology Groups

The homology groups of a space can be understood as a representation of the k-dimensional holes in that space. A k-th dimensional hole in space can be understood as follows: 0-dimensional holes represent connected components, 1-dimensional holes represent loops or cycles, 2-dimensional holes represent voids or empty volumes, and so on. The notion of homology and holes can be formalized more precisely using algebra and simplicial complexes. First, the *boundary* of any k-dimensional simplex can be expressed as the alternating sum of its (k-1) simplices; this is called the *boundary operator*, δ:

$$\delta((v_0, v_1, v_2, \ldots, v_k)) = \sum_{i=0}^{k} (-1)^i (v_0, v_1, \ldots, \bar{v_j}, \ldots, v_k)$$

, where $\bar{v_j}$ means the simplex v_j is removed.

Referring back to Figure 2, the boundary of the 2-dimensional simplex *(t1,t2,t3)* would be *(t2,t3)-(t1,t3)+(t1,t2)*, which could further be broken down into *t2-t3-t1+t3+t1-t2 = 0*. That the boundary equals zero is no coincidence, in fact the boundary equals 0 only when there is a loop/cycle in the shape. Computing the boundary of the square, we would also get 0. Hence examining all the *chains* in a simplicial complex, i.e. all possible linear combinations of simplices, the chains which map to 0 under the boundary operator are loops/cycles in the complex - formally, this is known as the *kernel* of the boundary operator.

However, the cycle in the square and the cycle in the triangle are distinguishable - the cycle in the triangle forms a 2-dimensional simplex, while the cycle in the square does not; formally this can be expressed as the triangle existing in the *image* space of the boundary operator at the next highest dimension, while the square would remain in the kernel space. And so the "holes" described earlier are in fact just cycles in the simplicial complex which do not belong to a higher dimensional simplex; the k-th homology group is the quotient space defined by:

$$H_k = \frac{Ker(\delta_k)}{Im(\delta_{k+1})}$$

2 Computational Background

2.1 Computing Persistent Homology

Given a point cloud of data, one feature we may to extract are the number of holes present in the data. One method is to construct a set of simplicial complexes (a *filtration* - an ordered set of simplicial complexes, each one a subset of the next) over various resolutions of the space and determine which holes *persist*: this is persistent homology.

The process can be broken down into 3 stages: creation of a filtration of simplicial complexes, construction & reduction of boundary matrices, and finally extracting homology intervals [3].

2.1.1 Vietoris-Rips Filtrations

The Vietoris-Rips filtration considering an open ball of radius ϵ centered at each point of the data; points which are within 2ϵ of each other are connected and form edges in the simplicial complex, X_ϵ. If $\epsilon_2 > \epsilon_1$, the simplices in $X_{\epsilon 2}$ will also be in $X_{\epsilon 1}$, and so we create a filtration of simplicial complexes (Figure 3):

$$X_{\epsilon 0} \subseteq X_{\epsilon 1} \subseteq X_{\epsilon 2} \subseteq \ldots \subseteq X_{\epsilon n}$$

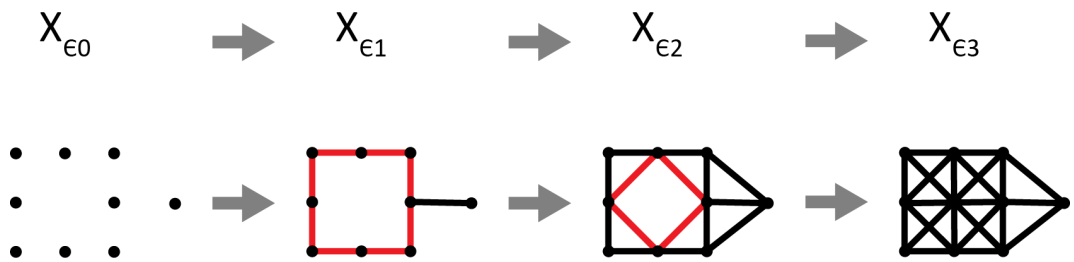

Figure 3: Example of a Vietoris-Rips filtration; a persistent "hole" is highlighted in red

To create a Vietoris-Rips filtration, the distance between all possible combinations of pairs of points must be computed to find the edges in the complex; that is for N points, a total of $\frac{N(N-1)}{2}$ operations must be performed. The higher n-dimensional simplices in the complex can then be found by either computing the mutual distances between all possible combinations of $n-1$ points, or by comparing the existing (n-1)-dimensional simplices; the former is convenient when N is relatively small as a single function suffices for detecting all simplices, however if N is large the latter method should be used for efficiency.

2.1.2 Boundary Matrices

Of note is that the filtration is not only a list of simplices but also the distance (ϵ) at which the simplex forms. In fact, we can systematically construct the filtration so that it is ordered as follows:

- a simplex appears in the list only after all of its faces have appeared
- a simplex formed at ϵ_i will appear earlier than a simplex formed at ϵ_j, if $\epsilon_i < \epsilon_j$

As such we can construct a *boundary matrix*, Δ, describing the formation of simplices for our filtration as follows:

1. Create an $N \times N$ matrix of zeros, where N is the total number of simplices in the filtration
2. For each simplex Δ_i, check if it is the face of any subsequent simplex Δ_j in the filtration (i.e. $i < j$); if so, set (i, j) entry of the matrix to 1

2.1.3 Homology Intervals

The next step is to reduce the boundary matrix (using the "standard" Algorithm 1), and read the intervals from the matrix describing when a "hole" appears or gets closed in the complex (e.g. the interval $[\varepsilon_1, \varepsilon_3)$ from Figure 3). Essentially, the standard algorithm traverses the columns of the boundary matrix from left to right; if the pivot entry in a column is also the pivot entry in a previous column, the previous column is added to the current column (note the boundary matrix is binary so adding pivots will result in a 0). Once all columns are traversed, the matrix is reduced and the intervals of finite holes can be interpreted from the pivot indices such that if (i, j) is a pivot entry, a hole is formed with the entry of simplex i in the filtration and is closed with the entry of simplex j.

2.2 Topological Approximation via Witness Complexes

Often the number of data points in a point cloud are so large that the computation of the filtration and boundary matrix operations to compute persistent homology become unrealistic; as such the point cloud may be reduced while maintaining its topological properties using a "witness complex" [5]. The point cloud can be reduced to a number of landmark points which are chosen inductively:

1. The first point is chosen randomly
2. Subsequent points are chosen by maximizing the minimum distance to all other landmark points

2.3 Wasserstein Distance

Once a set of homology intervals have been computed as outlined in 2.1.3), two different point clouds might be compared by comparing their homology intervals; this notion can be quantified using the *Wasserstein distance* between the intervals [6]. The intervals themselves can be embedded in the plane as (x,y) coordinates, where x is the ε at which the hole forms and y is the ε at which the hole closes. The Wasserstein distance between the two sets of intervals can then be found by:

1. Project each set of intervals onto the diagonal (e.g. blue set and red set in Figure 4)
2. Append the projection of each set of intervals onto the other set of intervals
3. Compute the distance between the two augmented sets of intervals and find an optimal pairing of points such that the total distance between points is minimal; each point can therefore only be paired with a point in the other set or to its own projection on the diagonal

Step 3 is an example of an assignment problem from linear optimization; the solution to such a problem can be solved using the "Hungarian" Algorithm 2.

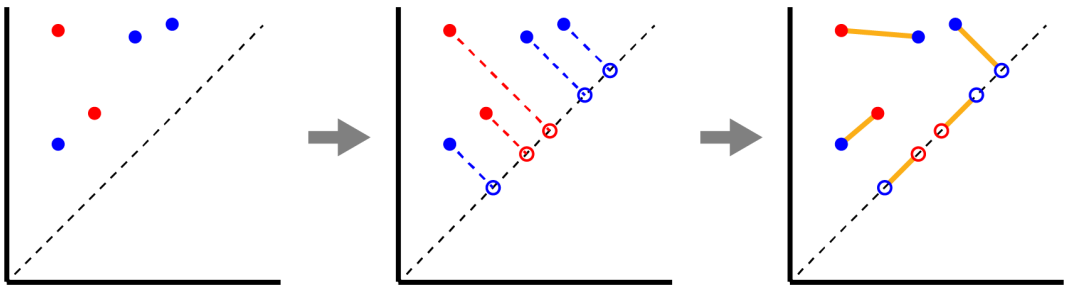

Figure 4: Steps to compute the Wasserstein distance between homology intervals embedded in $\mathbb{R}^2$

3 Methods

3.1 Dataset

The hip and knee joint angles and angular velocities from 5 performances of a run were collected from publicly available video provided by Southern Methodist University's Locomotor Performance Lab

(https://www.youtube.com/user/LocomotorLabSMU/). Two performances were of sprinters, two performances were of marathon runners and the last performance was from a paralympic sprinter. The videos were modulated so that stride frequency was consistent across performances - in this way the actual movement patterns could be distinguished between performances. The time series of joint angles and angular velocities lasted one gait cycle of the right leg, from foot strike to foot strike. The videos of performances and time series data is available at: https://github.com/abdulzaf/PHY407/tree/main/Data; the data is organized so that the columns 1-4 are in the following order: hip angle, hip angular velocity, knee angle, knee angular velocity.

All algorithms and analysis procedures were implemented in Python and are available at: https://github.com/abdulzaf/PHY407/tree/main/Python_Main
A set of test cases to ensure code functionality is also available at: https://github.com/abdulzaf/PHY407/tree/main/Testing

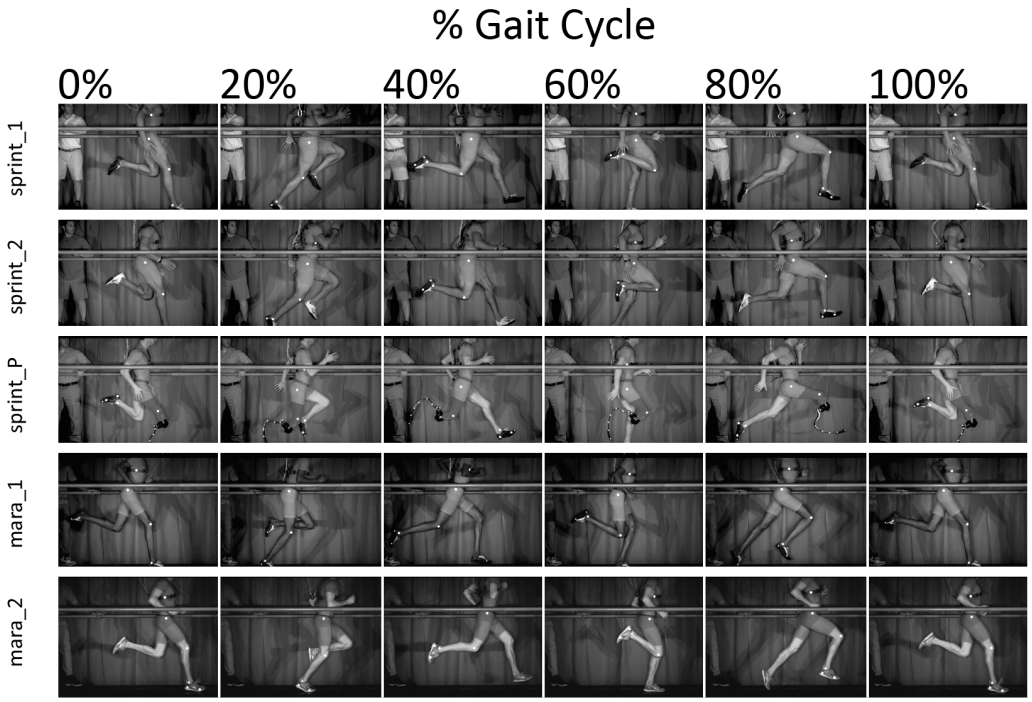

Figure 5: Image stills at 0%, 20%, 40%, 60%, 80% and 100% of gait cycle across all trials. sprint_1/sprint_2 are sprinters, sprint_P is a paralympic sprinter, mara_1/mara_2 are marathon runners

3.2 Continuous Relative Phase Analysis

First, the phase spaces of the hip and knee were constructed using their respective angles and angular velocities. The spaces were then normalized using a linear map taking the minimum to -1, and the maximum to +1, as follows [1]:

$$x_{norm}(t_i) = 2\left(\frac{(x(t_i) - min(x(t))}{max(x(t)) - min(x(t))}\right) - 1$$

The continuous relative phase of the athletes' gaits were computed using the procedure outlined in 1.2, by first computing the phase angle time series of both hip and knee, and then taking the difference to obtain a single time series of CRP angle:

$$CRP(t_i) = arctan(\frac{\dot{hip}_{norm}(t_i)}{hip_{norm}(t_i)}) - arctan(\frac{\dot{knee}_{norm}(t_i)}{knee_{norm}(t_i)})$$

3.3 Clustering Gait Patterns

First, a CRP phase space was constructed using the CRP angles calculated and the CRP angular velocity. The CRP angular velocity was computed with forward/backward difference schemes on the boundaries

of the CRP angle set, and a centred difference scheme on the interior of the CRP angle set.

The CRP phase spaces were normalized as in the previous section, with a small modification:

$$x_{norm}(t_i) = 2\left(\frac{(x(t_i) - min_{all}(x(t))}{max(x_{all}(t)) - min_{all}(x(t))}\right) - 1$$

That is, the maximum and minimum across all performances were used in the normalization; in this way the shape of the phase spaces relative to each other was preserved, while also bringing all spaces into the range [-1,1]. The point clouds of the phase spaces were down-sampled using a witness complex of 10 landmark points, for the sake of computation speed (Figure 6).

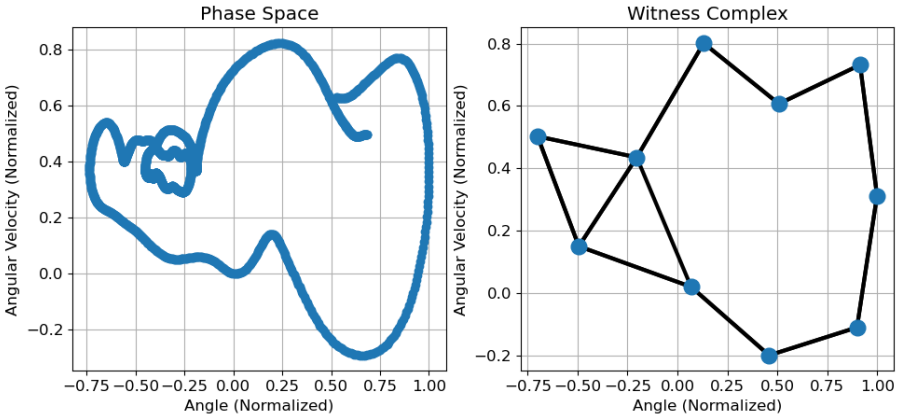

Figure 6: The downsampling of the phase space point cloud using a witness complex with 10 landmark points

Next, the loops/holes in the phase space were found by computing the persistent homology of the phase space, as outlined in 2.1. The Vietoris-Rips complex using ϵ in the range of 0 to 3, in steps of 0.01; that is the final complex in the filtration should be a complete graph on 10 vertices, i.e. all the holes should have been covered (Figure 7).

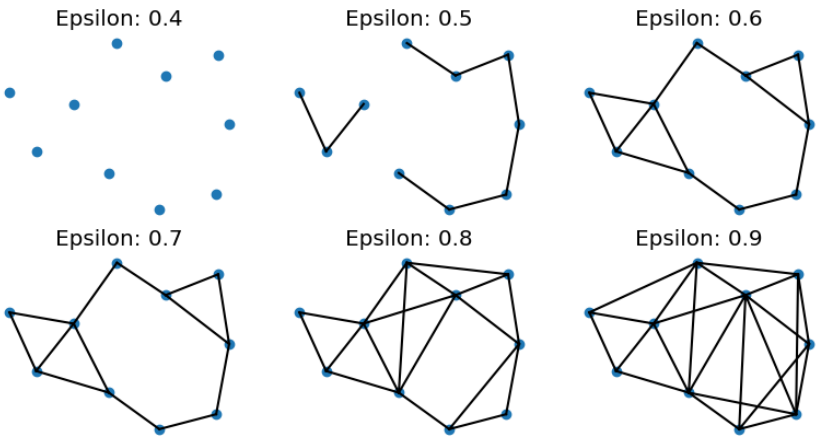

Figure 7: Selected steps in the Vietoris-Rips filtration on the witness complex of the CRP phase space

Once the homology intervals were computed, the 3 largest intervals were used to represent the principal loops in the phase space. The Wasserstein distance between intervals for different performances was used to create a distance matrix, D. The distances were then normalized based on the maximum

distance (i.e. dividing the matrix entries of D by the maximum distance to bring values into a range of 0 to 1) and then an adjacency matrix, A, was created by using a distance threshold of 0.5 (i.e. entries in A are 1 if the corresponding entry in D is < 0.5, and 0 otherwise).

4 Results & Analysis

4.1 Results

The following are plots of the continuous relative phase angle plotted against the % of gait complete and the CRP phase space for all 5 performances:

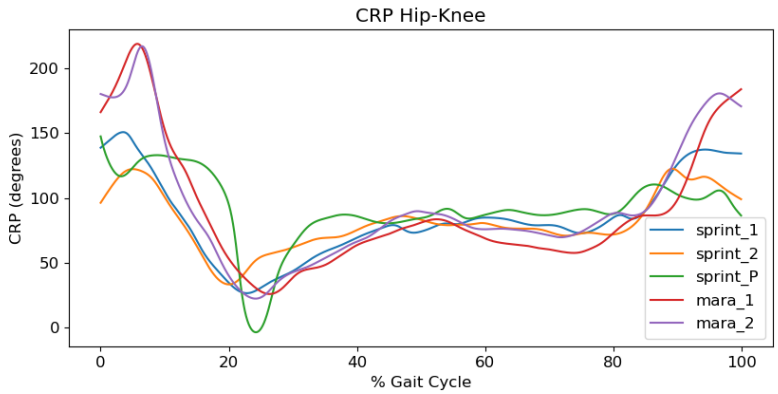

Figure 8: CRP angle versus % gait cycle complete

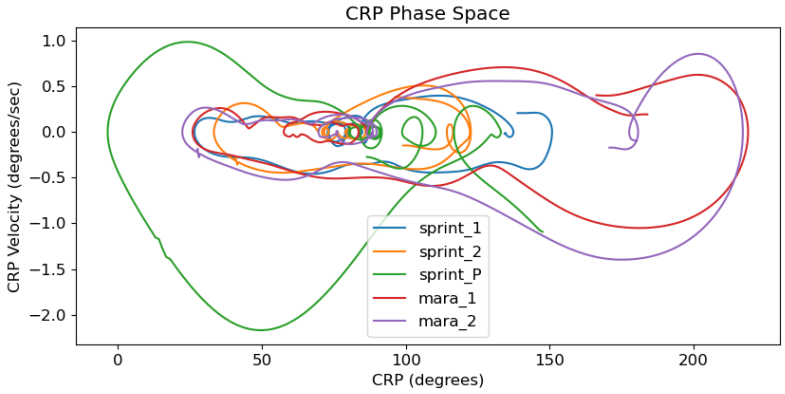

Figure 9: CRP Phase Space: CRP angular velocity (y) versus CRP angle (x)

The following are plots of the homology intervals as a persistence diagram and the Wasserstein distance matrix with its corresponding thresholded adjacency matrix:

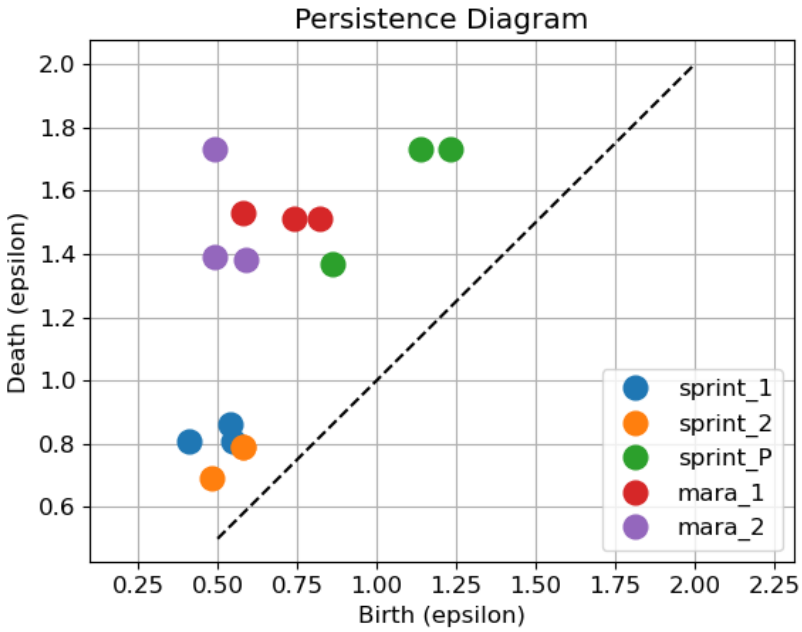

Figure 10: Persistence diagrams for homology intervals with index of closing (y) versus index of formation (x)

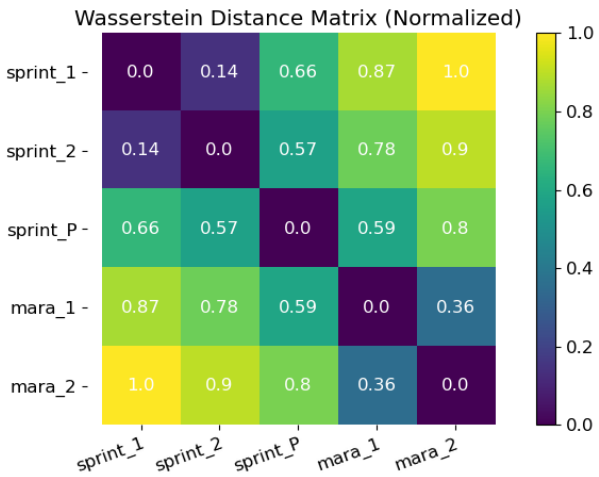

Figure 11: Normalized Wasserstein distance between persistence diagrams

Figure 12: Corresponding adjacency matrix for Figure 11 with threshold=0.5

4.2 Analysis

From visual inspection of the CRP plots of Figure 8 the profiles of the CRP time series indicate some differences between types of performances, yet the differences become much more apparent when plotted in the phase space as in Figure 9. In the phase space, both sprint performances (*sprint_1* and *sprint_2*) form a tight limit cycle, the marathoners (*mara_1* and *mara_2*) form an elongated cycle and the paralympic sprinter (*sprint_P*) forms a large loop in the opposite end of the phase space compared to the marathoners.

An inspection of the persistence diagrams in Figure 10 reveals that in fact all 5 sprints have two different sized limit cycles - they all exhibit dual periodicity; this is from the two clusters of points appearing for each performance at different indices in the filtration. Notably, the sprinters' cycles are

much closer together due to the tighter profile in the phase space (and are possibly even constitute the same cycle), the marathoners cycles are slightly more distinct, while the paralympic sprinter demonstrates the largest disparity in cycle size. Corresponding to the visual intuition from Figures 8 & 9, the profiles of similar types of performances are also similar in the persistence diagram.

Finally, Figures 11 & 12 display the actual (normalized) distance values between performances and their connection based on a 50% threshold; from the adjacency matrix, the sprint performances are linked with each other, the marathon performances are linked with each other and the paralympic sprinter's performance is disconnected from all the others.

5 Discussion

The method above of applying topological concepts to dynamical systems theory and biomechanics proves useful to distinguish between movement patterns which may otherwise be invisible to even a trained eye. One might wonder whether the approach may be simplified: for example, why not apply the Wasserstein distance directly to the phase space point clouds in order to distinguish between them? In fact, such analyses have been performed on gait, using Geometric Template Matching rather than the Wasserstein distance [8]. However, since these applications only concern themselves with the clustering of similar gait types, the underlying reasons of *why* the gaits are different cannot be extracted. The value from a coaching or clinical purpose comes from being able to pinpoint what the differences in movement patterning are. Therefore there is added value in actually extracting features of the phase space like the size of limit cycles as found via persistent homology; that the homology groups are able to distinguish and cluster differences in gait is an added bonus.

Regarding the size of the limit cycles, it must be emphasized the differences in limit cycles are results of differences in hip-knee coordination, rather than simply speed of movement as all motions were time modulated in order to have the same stride frequency. Therefore that the sprinters' gaits should have a smaller cycle in the relative phase space compared to the marathoners' gaits cannot be merely explained by the differences in stride frequency. The actual meaning of the smaller limit cycle implies that there is a smaller range of CRP angles between hip and knee in sprinting, meaning in comparison to the other runs the sprinters hips and knees maintained a more stable relative phase (i.e. coordination pattern) for the majority of the gait cycle. By comparison, the gaits of the marathon runners and the paralympic sprinter exhibited a more noticeable double limit cycle, where the hip-knee system was more in-phase for one cycle compared to the other. Referring to Figures 8 & 9, the variable phase moments for the paralympic sprinter occur about 20%-40% into the stride, that is just between toe off and heel recovery (see Figure 5); this may be a result of the shape of the running blade a) introducing extra dynamics at toe off due to the different elastic properties of the blade versus a human shank & foot, as well as b) impeding heel recovery.

Regarding the analysis methods, of note is that there are no set rules for setting parameters for the topological approach; that is, the start or stop points of the filtration, the number of landmark points in the witness complex approximation, or the number of intervals to consider when computing the Wasserstein distance are all heuristics and entirely context dependant. There are very broad guidelines for some of these metrics, for example the number of landmark points should be at least 20x fewer than the original point cloud [5]. For other metrics, such as which intervals to consider "persistent" and which to consider noise, entropy based criteria have been explored [9]. In any case, the actual parameter values are not fixed, but vary based on context and sometimes can even be difficult to justify given the abstract notion of spaces involved. A good test is to perturb parameters slightly to see if results are stable. For example, the analysis above used the 3 longest intervals to compute the Wasserstein distances, but increasing this parameter anywhere from 4 to 10 (and possibly more) intervals, i.e. introducing more noise, produces the same clustering result; thus there can be some degree of confidence in the results.

6 Conclusion

The computation of the persistent homology of the phase space in biomechanics can be used to quantify and distinguish different coordination patterns occurring across performances. Care must be taken to choose parameters for the analysis which present stable results but are also computationally feasible due to the possibility of high-dimensional data. Finally, there is still much more work involved to transform the homologies into actionable insight for practitioners; knowing limit cycles are larger or smaller gives some abstract intuition about differences in movement patterns however much more concrete relations to

the actual body poses is required. In this sense, the homologies are a first step, and must be augmented with the detection of other attractors in the phase space which can then be mapped back to the original movement via time indexing to identify moments of stability/variability/compensation/forcing/etc, which are present.

References

[1] Lamb, P. F., & Stöckl, M. (2014). On the use of continuous relative phase: Review of current approaches and outline for a new standard. Clinical Biomechanics, 29(5), 484–493. https://doi.org/10.1016/j.clinbiomech.2014.03.008

[2] Wikimedia Foundation. (2020, December 1). Homology (mathematics). Wikipedia. https://en.wikipedia.org/wiki/Homology_(mathematics).

[3] Otter, N., Porter, M. A., Tillmann, U., Grindrod, P., &; Harrington, H. A. (2017). A roadmap for the computation of persistent homology. EPJ Data Science, 6(1). https://doi.org/10.1140/epjds/s13688-017-0109-5

[4] Zomorodian, A., & Carlsson, G. (2004). Computing persistent homology. Proceedings of the Twentieth Annual Symposium on Computational Geometry - SCG '04. https://doi.org/10.1145/997817.997870

[5] Silva, Vin & Carlsson, Gunnar. (2004). Topological estimation using witness complexes. Proc. Sympos. Point-Based Graphics. https://10.2312/SPBG/SPBG04/157-166.

[6] Kerber, M., Morozov, D., & Nigmetov, A. (2015). Geometry Helps to Compare Persistence Diagrams. 2016 Proceedings of the Eighteenth Workshop on Algorithm Engineering and Experiments (ALENEX). https://doi.org/10.1137/1.9781611974317.9

[7] Date, K., & Nagi, R. (2016). GPU-accelerated Hungarian algorithms for the Linear Assignment Problem. Parallel Computing, 57, 52–72. https://doi.org/10.1016/j.parco.2016.05.012

[8] Frank, Jordan & Mannor, Shie & Precup, Doina. (2010). Activity and Gait Recognition with Time-Delay Embeddings.

[9] Atienza, N., Gonzalez-Diaz, R., & Rucco, M. (2016). Separating Topological Noise from Features Using Persistent Entropy. Software Technologies: Applications and Foundations Lecture Notes in Computer Science, 3–12. https://doi.org/10.1007/978-3-319-50230-4_1

APPENDIX I: Algorithms

Algorithm 1 Standard algorithm for reducing a boundary matrix [4]

Require: $\delta \longrightarrow$ boundary matrix

for $column_i$ in δ **do**
  if pivot($column_i$)==pivot($column_j$), $j < i$ **then**
    $column_i$ += $column_j$
  end if
end for

Algorithm 2 Hungarian Algorithm for Linear Assignment Problem [7]

Require: $CostMatrix \longrightarrow$ an $N \times N$ square cost matrix

for row_i in CostMatrix **do**
  row_i −= $minimum(row_i)$
end for
for $column_i$ in CostMatrix **do**
  $columm_i$ −= $minimum(row_i)$
end for

lines = minimum number of lines to cover all zeros in CostMatrix
while $lines < N$ **do**
  a = minimum uncovered number in CostMatrix
  for row_i in CostMatrix **do**
    if row_i is uncovered **then**
      row_i −= a
    end if
  end for
  for $column_i$ in CostMatrix **do**
    if $column_i$ is covered **then**
      $column_i$ += a
    end if
  end for
  lines = minimum number of lines to cover all zeros in CostMatrix
end while